

ACKNOWLEDGMENTS

Supported by U.S. Department of Energy award DE-EE0006709 (solar cell) and Defense Threat Reduction Agency award HDTRA1-14-1-0030 (radiation detector). J.H. conceived the idea and supervised the project; Q.D. grew the single crystals and fabricated the devices; Q.D., Y.F., and Y.S. conducted the electric and optical characterization of the devices;

P.M., J.Q., and L.C. measured the devices under gamma ray irradiation and did the simulation; and J.H. wrote the paper.

SUPPLEMENTARY MATERIALS

www.sciencemag.org/content/347/6225/967/suppl/DC1
Materials and Methods

Figs. S1 to S11
Tables S1 and S2
References (17–21)

27 December 2014; accepted 20 January 2015
Published online 29 January 2015;
10.1126/science.aaa5760

WATER SPLITTING

Metal-free efficient photocatalyst for stable visible water splitting via a two-electron pathway

Juan Liu,¹ Yang Liu,¹ Naiyun Liu,¹ Yuzhi Han,¹ Xing Zhang,¹ Hui Huang,¹ Yeshayahu Lifshitz,^{1,2*} Shuit-Tong Lee,^{1,*} Jun Zhong,¹ Zhenhui Kang^{1*}

The use of solar energy to produce molecular hydrogen and oxygen (H₂ and O₂) from overall water splitting is a promising means of renewable energy storage. In the past 40 years, various inorganic and organic systems have been developed as photocatalysts for water splitting driven by visible light. These photocatalysts, however, still suffer from low quantum efficiency and/or poor stability. We report the design and fabrication of a metal-free carbon nanodot–carbon nitride (C₃N₄) nanocomposite and demonstrate its impressive performance for photocatalytic solar water splitting. We measured quantum efficiencies of 16% for wavelength $\lambda = 420 \pm 20$ nanometers, 6.29% for $\lambda = 580 \pm 15$ nanometers, and 4.42% for $\lambda = 600 \pm 10$ nanometers, and determined an overall solar energy conversion efficiency of 2.0%. The catalyst comprises low-cost, Earth-abundant, environmentally friendly materials and shows excellent stability.

Production of hydrogen and oxygen from water is a promising means of storing solar energy in a way that compensates for the intermittency of sunlight as a primary source of power (1, 2). It can be realized by applying a hybrid system in which a solar cell powers an electrolyzer [photovoltaic (PV) electrolysis]. Photoelectrolysis (PE) uses photocatalyst electrodes with additional electrical power provided by a photovoltaic element. Photocatalysis (PC) involves light-irradiated catalysts (typically catalyst powders suspended in water) for water splitting (3). Recently reported “solar-to-hydrogen” (STH) efficiencies for PV electrolysis systems exceed 10% (4–6). State-of-the-art PE systems yield STH values of 2 to 3% (7) but are believed to provide a cheaper solution for H₂ production. PC is the simplest water-splitting approach, more amenable to cheap, large-scale applications of H₂ generation. Unfortunately, despite intense efforts during the past 40 years (8–15), current direct photocatalysts for water splitting still face several challenging issues: (i) Currently reported catalysts suffer from low quantum efficiency (QE) in the visible range, with STH efficiencies less than

0.1% (16–18); (ii) many photocatalysts are made of rare and expensive materials; (iii) various photocatalysts show poor stability [e.g., inorganic sulfide and (oxy)nitride-based photocatalysts are less stable and more susceptible to oxidation than water]; (iv) O₂ release from semiconductor catalysts is difficult, so that the use of sacrificial reagents is required; (v) the overall four-electron water oxidation to O₂ encounters a large overpotential; and (vi) the kinetically competing two-electron reaction to H₂O₂ often poisons the photocatalysts (19).

Overall water splitting to H₂ and O₂ requires a high free energy of 113.38 kcal/mol (20, 21). The challenge lies mainly in the release of diatomic O₂, which involves four electron and four proton transfers for the eventual formation of an O–O bond. The concerted four-electron process for oxygen evolution (1.23 eV) is thermodynamically more favorable than the two-electron process for H₂O₂ formation (1.78 eV). However, detailed analysis (see supplementary text) shows that a higher reaction rate may be achieved in a system where water is first oxidized via a two-electron reaction to H₂O₂ and H₂, followed by H₂O₂ decomposition to O₂ and H₂O. For this stepwise two-electron/two-electron water splitting to H₂ and O₂ to be viable and practical, the photocatalyst applied should be capable of promoting generation as well as subsequent decomposition of H₂O₂ with high efficiencies and low overpotentials, so as to allow considerable reduction in the energy cost for production of H₂ and O₂

via overall water splitting. Here, we report that nanocomposites of carbon nanodots embedded in a C₃N₄ matrix perform as an excellent photocatalyst fulfilling the above requirements.

C₃N₄ is commercially available (e.g., from Carbo-deon) and can be easily fabricated (e.g., from urea) (19). It is an Earth-abundant and low-cost photocatalyst capable of generating H₂ and H₂O₂ from water even in the absence of catalytic metals, albeit with a low QE (19, 22–26). C₃N₄ belongs to the oldest reported polymer materials prepared by chemists (by Berzelius in ~1830) and first termed “Melon” (27). In 2006 it was determined that the visible light activity of TiO₂ after treatment with urea was due to “Melon” (28). In 2009, Antonietti and colleagues described in detail the optical properties, electronic structure, and photocatalytic activity of C₃N₄ (29). Following this work, many groups attempted to optimize the catalytic properties of C₃N₄, motivated by its relatively low band gap energy E_g of 2.7 eV, and high valence band and conduction band positions (29) [1.8 and –0.9 eV versus reversible hydrogen electrode (RHE)]. Many heterojunction composites with oxide semiconductors as well as photocatalyst systems were investigated. The latter included systems with a variety of oxides (30) and sulfides (31) along with pure metals (19) and even graphene (32) and carbon nanotubes (33). Different preparation methods were studied in an effort to increase the surface area of C₃N₄ and to improve its catalytic activity. The QE values obtained using C₃N₄ as a catalyst for water splitting to H₂ and O₂ have been low (maximum 3.75% at 420 nm and less than 0.5% for 500 nm), and generally the use of a sacrificial reagent has been necessary (19, 24, 26, 30–32, 34). The efficiency at 700 nm can be largely increased by applying dye molecules, but again a sacrificial reagent is a must (35). During water splitting C₃N₄ suffers from poisoning by the produced H₂O₂, which is difficult to remove from the C₃N₄ surface (19). Different methods including stirring, bubbling, and/or addition of chemical agents have been attempted for regeneration of the poisoned C₃N₄ catalyst (19).

Carbon nanodots (CDots; monodisperse graphite particles less than 10 nm in diameter) exhibit unique photo-induced electron transfer, photoluminescence, and electron reservoir properties (36). In particular, CDots possess high catalytic activity (by chemical catalysis; no light is needed) for H₂O₂ decomposition (37). Given the photocatalytic properties of CDots and C₃N₄, we hypothesized that a combination of CDots and C₃N₄ could constitute a high-performance composite photocatalyst for water splitting via the stepwise two-electron/two-electron process: (i) 2H₂O → H₂O₂ + H₂; (ii) 2H₂O₂ → 2H₂O + O₂.

¹Jiangsu Key Laboratory for Carbon-based Functional Materials and Devices, Institute of Functional Nano and Soft Materials (FUNSOM), Soochow University, Suzhou 215123, China. ²Department of Materials Science and Engineering, Technion, Israel Institute of Technology, Haifa 3200003, Israel. *Corresponding authors. E-mail: zhikang@suda.edu.cn (Z.K.); apannale@suda.edu.cn (S.-T.L.); shayli@tx.technion.ac.il (Y.L.)

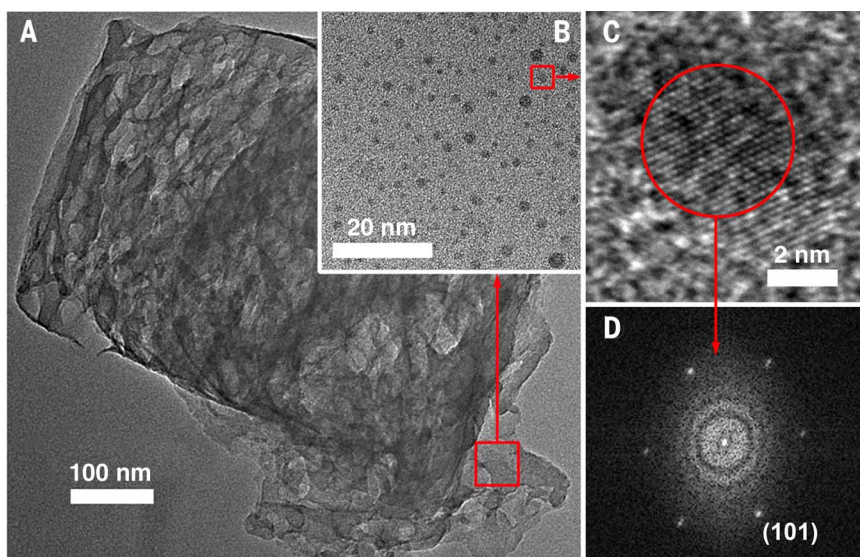


Fig. 1. Characterization of the physical structure of the composite catalyst. (A) TEM image of a grain of the CDots- C_3N_4 composite. (B) A magnified TEM image of the CDots- C_3N_4 region of (A) marked in red. (C) HRTEM image of a single CDot embedded in C_3N_4 . (D) Corresponding FFT pattern of the crystallite in (C), indicating hexagonal symmetry. In all panels, the CDots concentration of the sample was $1.6 \times 10^{-5} g_{CDots}/g_{catalyst}$.

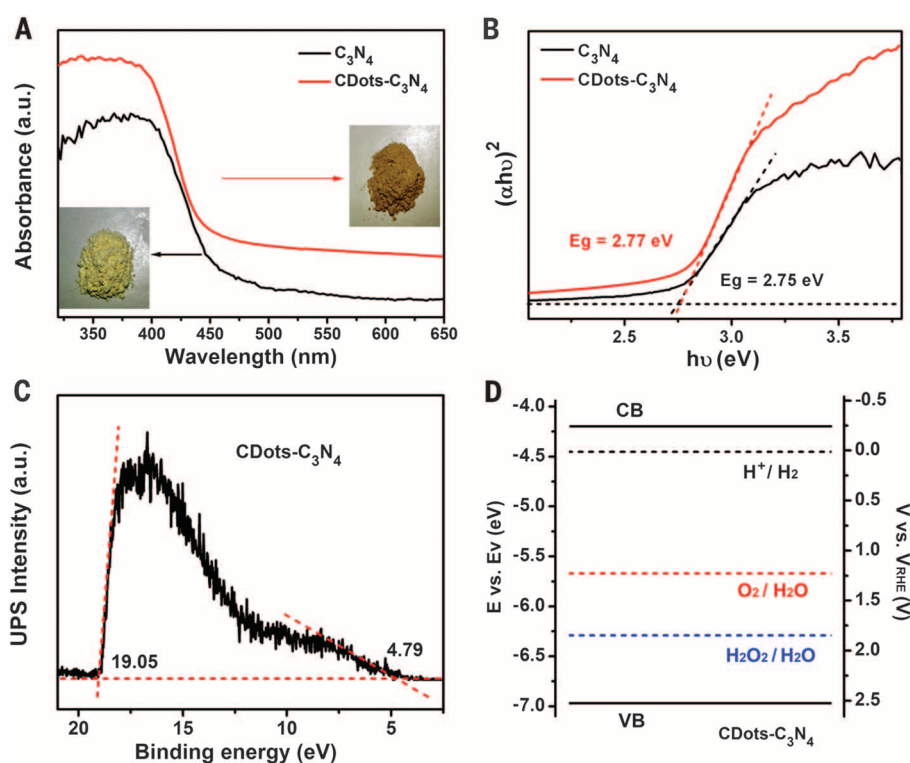


Fig. 2. Characterization of the electronic structure of the composite catalyst. (A) UV-vis absorption spectra of C_3N_4 (black curve) and CDots- C_3N_4 (red curve) catalysts. Inset: Digital photograph of catalyst grains. The actual size of the digital photo is 4 cm \times 4.3 cm. (B) $(\alpha h\nu)^2$ versus $h\nu$ curve of C_3N_4 (black curve) and CDots- C_3N_4 (red curve). The horizontal dashed black line marks the baseline; the other dashed lines are the tangents of the curves. The intersection value is the band gap. (C) UPS spectra of CDots- C_3N_4 (black curve). The dashed red lines mark the baseline and the tangents of the curve. The intersections of the tangents with the baseline give the edges of the UPS spectra from which the UPS width is determined. (D) Band structure diagram for CDots- C_3N_4 . In all panels, the CDots concentration in the CDots- C_3N_4 sample analyzed was $1.6 \times 10^{-5} g_{CDots}/g_{catalyst}$. VB, valence band; CB, conduction band.

CDots were synthesized by a typical electrochemical method followed by hydrothermal treatment with ammonia (37). CDots- C_3N_4 composites were then prepared by heating a mixture of ammonia-treated CDots and urea powder at 550°C for 3 hours (see supplementary material). Characterization of the as-produced CDots- C_3N_4 composites by transmission electron microscopy (TEM) showed highly porous grains (Fig. 1A) consisting of CDots (2 to 10 nm in diameter) embedded in a porous C_3N_4 matrix (Fig. 1B). The CDots were non-uniformly distributed, with apparent regions of dots denser by one order of magnitude than the average concentration in the C_3N_4 matrix. A high-resolution TEM (HRTEM) image of a CDot crystallite (Fig. 1C) showed an interplanar spacing of 0.202 nm, which corresponds to the $\langle 101 \rangle$ spacing of graphitic carbon. The corresponding 2D fast Fourier transform (FFT) pattern (Fig. 1D) exhibits the hexagonal crystalline structure of the CDots. Linewidth analysis of x-ray powder diffraction patterns (fig. S1) of the grains of the CDots- C_3N_4 composite suggests that the C_3N_4 matrix comprises nanocrystallites with an average diameter of ~ 4 nm (29, 38, 39). The diameter of the grains of the CDots- C_3N_4 composite deduced from atomic force microscopy (fig. S2) ranges between 90 and 400 nm (fig. S3).

The incorporation of CDots into the C_3N_4 matrix leads to an increase in the ultraviolet-visible (UV-vis) absorption over the entire wavelength range investigated (Fig. 2A). The optical band gap of a semiconductor can be estimated from the Tauc plot [i.e., the curve of converted $(\alpha h\nu)^r$ versus $h\nu$ from the UV-vis spectrum, in which α , h , and ν are the absorption coefficient, Planck constant, and light frequency, respectively, and $r = 2$ for a direct band gap material and $r = 1/2$ for an indirect band gap material]. Figure 2B shows a good linear fit when using $r = 2$, in accord with previous work (25) claiming C_3N_4 to be a direct band gap material (no good linear fit is obtained for $r = 1/2$). The E_g value of CDots- C_3N_4 (CDots concentration of $1.6 \times 10^{-5} g_{CDots}/g_{catalyst}$) was thus determined to be 2.77 eV by measuring the x -axis intercept of an extrapolated line from the linear regime of the curve (Fig. 2B, red curve), which is almost identical to that of pure C_3N_4 (Fig. 2B, 2.75 eV, black curve) within experimental error. The Tauc plot curve (Fig. 2B, red curve) of CDots- C_3N_4 shows an apparent tail between 2.0 and 2.7 eV, which is helpful for improving the light absorbance and the photocatalytic efficiency. Aside from an appropriate band gap, the proper matching of conduction band and valence band levels of a photocatalyst with the redox potentials of the photocatalytic reactions is also important for water splitting. We used ultraviolet photoelectron spectroscopy (UPS) to determine the ionization potential [equivalent to the valence band energy (E_v)] of CDots- C_3N_4 , which was calculated to be 6.96 eV by subtracting the width of the He I UPS spectra (Fig. 2C) from the excitation energy (21.22 eV). The conduction band energy E_c is thus estimated at 4.19 eV from $E_v - E_g$. The E_g , E_v , and E_c values of

CDots-C₃N₄ in electron volts are converted to electrochemical energy potentials in volts according to the reference standard for which 0 V versus RHE (reversible hydrogen electrode) equals -4.44 eV versus vac (vacuum level). Figure 2D further shows that the reduction level for H₂ is positioned below the conduction band of CDots-C₃N₄, and the oxidation level for H₂O to H₂O₂ or O₂ is above the valence band; these bands are properly positioned to permit transfer of electrons and holes, respectively, for water splitting, thus corroborating the potential of CDots-C₃N₄ as a photocatalyst for overall water splitting. Additional characterization of the CDots-C₃N₄ composites included Raman spectroscopy (fig. S4), Fourier transform infrared spectroscopy (FTIR, fig. S5), energy-dispersive spectra (EDS, fig. S6), x-ray photoelectron spectroscopy (XPS, fig. S7), and x-ray absorption near edge structure (XANES, fig. S8).

Figure 3A shows the evolution of H₂ and O₂ from 150 ml of water containing 0.08 g of non-optimized CDots-C₃N₄ composite under visible light irradiation. H₂ and O₂ were both quantified by gas chromatography (GC); a typical sample curve (GC signal) is shown in fig. S9. H₂ and O₂ evolution proceeded continuously in a molar ratio of H₂/O₂ of 2.02, effectively identical to the theoretical value of 2 for overall water splitting, but ceased immediately when the light was turned off. The constant H₂ evolution rate was ~8.4 μmol/hour and that of O₂ ~4.1 μmol/hour, and no other gases than H₂ and O₂ (e.g., CO₂ or N₂) were detected by GC. Control experiments showed that no O₂ evolution was detected by gas chromatography when pure CDots, pure C₃N₄, or a macroscopic mixture of the two was used as photocatalyst over a 24-hour reaction period. This indicates (see supplementary material) that proximity between the CDots and the generation sites of H₂O₂ (achieved in the composite CDots-C₃N₄ structure) is necessary for the CDots to decompose H₂O₂ and generate O₂.

We further verified that the detected O₂ was indeed generated by water splitting. When we used H₂¹⁸O as reagent under the same water-splitting conditions described earlier, ¹⁸O₂ (mass 36) was the only product detected by GC-MS (gas chromatography-mass spectrometry). We next measured the QE of overall water splitting by CDots-C₃N₄ as a function of the incident light wavelength λ₀ (Fig. 3B). QE decreased with increasing wavelength, and the longest wavelength capable of inducing water-splitting coincided with the red absorption edge of the CDots-C₃N₄ composite, suggesting the reaction proceeds via photoabsorption by the catalyst. We proceeded to optimize the catalyst composition by measuring QE for different concentrations of CDots in a fixed mass of composite (Fig. 3C). With increasing CDots concentration, the QE increased to a maximum value of 16% around 4.8 × 10⁻³ g_{CDots}/g_{catalyst}, after which it decreased upon addition of more CDots. Next, we optimized the amount of composite catalyst added to water at the optimum CDots/C₃N₄ ratio of 4.8 × 10⁻³ g_{CDots}/g_{catalyst} (Fig. 3D). We found that the QE increased to a maximum value of 16% as the catalyst was

added, and then stayed the same upon further addition.

We interpret the dependence of QE on CDots concentration to an enhancement of the decomposition rate of H₂O₂ until the rate is sufficient to remove all the generated H₂O₂ (by the photocatalytic effect of C₃N₄). Afterward, further increase of the CDots concentration could enhance the light absorption by introducing subband states, thus raising the QE to a maximum, after which addition of more CDots seems to increase energy losses (light absorbed in CDots and not in C₃N₄, e⁻/h⁺ recombination, lower catalytic efficiency of C₃N₄ due to CDots, etc.), thus decreasing the QE. On the other hand, the initial increase (Fig. 3D) of the composite catalyst load (keeping the CDots concentration constant) increases the generation rate of H₂ (more catalyst → more light absorbance) until reaching a maximum. Additional increase of the composite CDots-C₃N₄ load cannot further increase the light absorbance (all incident light is absorbed), so that the QE remains unchanged (Fig. 3D). We believe

that the large values of QE obtained by the CDots-C₃N₄ composite relate to the highly porous structure of the C₃N₄ grains (resulting from the preparation method of the catalyst), which yields a large water-catalyst interface area [97 m²/g as measured by the Brunauer-Emmett-Teller (BET) method]. Our further studies systematically confirmed that water-splitting photocatalysis by CDots-C₃N₄ indeed proceeds via the stepwise 2e⁻/2e⁻ two-step process, in which H₂O oxidation to H₂O₂ is the first and rate-limiting step, followed by the second and fast step of H₂O₂ disproportionation to O₂, which is chemically catalyzed by CDots (detailed experiments and analysis are given in the supplementary material).

The experiments above focused on catalytic properties at λ = 420 nm; however, solar water splitting in the vicinity of the solar spectrum peak (λ = 550 to 650 nm) region is more relevant to efficient harvesting of solar energy. The QE of the standard CDots-C₃N₄ catalyst (i.e., CDots concentration of 1.6 × 10⁻⁵ g_{CDots}/g_{catalyst}, catalyst load 0.53 g/liter) at λ = 580 nm was relatively low

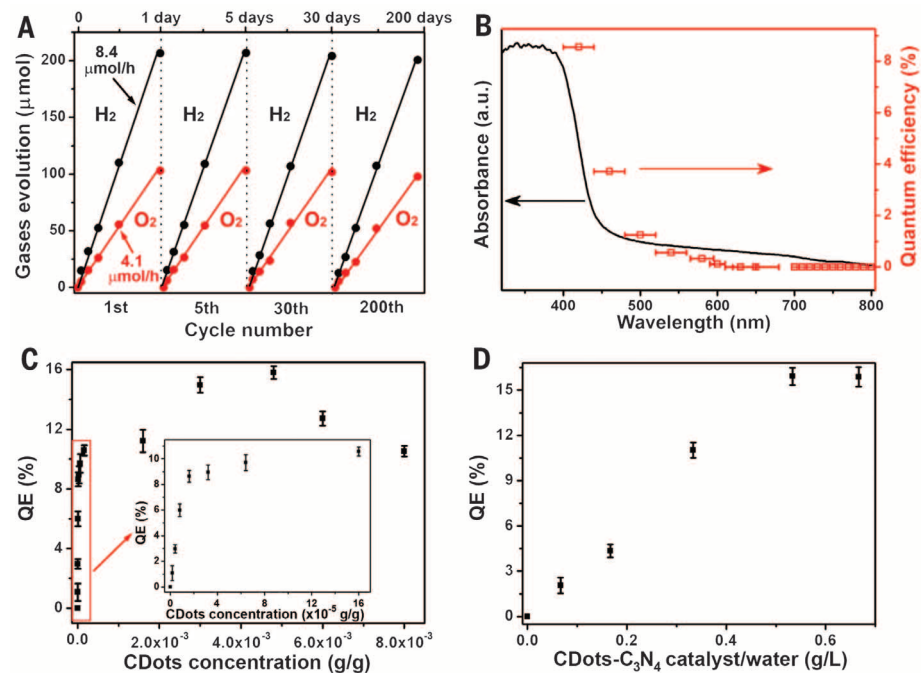


Fig. 3. Photocatalytic water-splitting performance of the composite catalyst. (A) Typical time course of H₂ and O₂ production from water under visible light irradiation (by a 300-W Xe lamp using a long-pass cutoff filter allowing λ > 420 nm) catalyzed by CDots-C₃N₄ (CDots concentration, 1.6 × 10⁻⁵ g_{CDots}/g_{catalyst}). (B) Wavelength-dependent QE (red dots) of water splitting by CDots-C₃N₄ (irradiated by a 300-W Xe lamp using a bandpass filter of λ ± 20 nm for 420, 460, 500, 540, and 630 nm; a bandpass filter of λ ± 15 nm for 580 nm; a bandpass filter of λ ± 10 nm for 600 nm; a bandpass filter of λ ± 30 nm for 650 nm; and a long-pass cutoff filter for λ > 700 nm). The UV-vis absorption spectrum (black) of the CDots-C₃N₄ catalyst is superimposed for comparison. The data were derived using a nonoptimized CDots-C₃N₄ catalyst (CDots concentration, 1.6 × 10⁻⁵ g_{CDots}/g_{catalyst}). (C) QE for different concentrations of CDots (g_{CDots}/g_{catalyst}) in a fixed mass of composite catalyst. Experimental conditions: 0.080 g of catalyst, 150 ml of ultrapure water, 300-W Xe lamp irradiation for 24 hours with a 420 ± 20 nm bandpass filter. The inset shows an enlarged curve of the low CDots concentration in the region marked in the figure. (D) QE for different catalyst loads with a constant CDots concentration of 4.8 × 10⁻³ g_{CDots}/g_{catalyst} in 150 ml of ultrapure water. The experiments were carried out under the same light irradiation conditions as in (C). For (B), the horizontal bars indicate the width of the wavelength band of the filters used. For (C) and (D), the vertical error bars indicate the maximum and minimum values obtained; the dot represents the average value.

($\sim 0.3\%$). Upon optimization, we succeeded in preparing catalysts with a high QE = 16% at $\lambda = 420 \pm 20$ nm by increasing the quantity of CDots in the C_3N_4 . The higher CDots concentration and the associated larger total C fraction in the composite (Fig. 4A) concurrently increased the absorbance in the solar spectrum peak region (black versus red curve in Fig. 4B). This is most likely due to the effect of C addition leading to the formation of more subband states in the band gap. Figure 4C shows that the H_2 generation rate at our standard conditions (80 mg of catalyst in 150 ml of water; 300-W Xe light radiation with a long-pass cutoff filter allowing $\lambda > 420$ nm) increased by a factor of 5.4 for CDots- C_3N_4 with a higher CDots concentration. The QE of the catalyst with the optimum amount of CDots (4.8×10^{-3} $g_{CDots}/g_{catalyst}$) remarkably increased (Fig. 4D, black) relative to the QE of the catalyst with a CDots concentration of 1.6×10^{-5} $g_{CDots}/g_{catalyst}$ (Fig. 4D, red). It reached 6.29% at $\lambda = 580 \pm 15$ nm (20 times the QE for the 1.6×10^{-5} $g_{CDots}/g_{catalyst}$ catalyst) and 4.42% at $\lambda = 600 \pm 10$ nm. For irradiation wavelengths $\lambda > 650$ nm, both catalyst systems showed zero QE (Fig. 4D).

The solar energy conversion was evaluated in the following studies by using an AM 1.5G (air mass 1.5 global conditions) solar simulator as the light source (see fig. S10 for ~output

spectral distribution) and CDots- C_3N_4 (4.8×10^{-3} $g_{CDots}/g_{catalyst}$) as the catalyst (80 mg catalyst in 150 ml of water). After 6 hours of illumination, the total incident power over the irradiation area of 9 cm^2 was 0.63 W, so that the total input energy was 1.36×10^4 J. During the photocatalytic reaction, 1150 μmol of H_2 was detected by GC, which indicated that the energy generated by water splitting is $E_F = 274$ J. The STH value of CDots- C_3N_4 with the higher concentration of CDots was determined to be 2.0%, which is at least one order of magnitude larger than previously reported values (40, 41). Indeed, the STH values were very low (0.3% for 1.6×10^{-5} $g_{CDots}/g_{catalyst}$) for low CDots concentration and reached 2% only at the optimum CDots concentration (fig. S11). An independent alternative STH calculation based on the CDots- C_3N_4 (4.8×10^{-3} $g_{CDots}/g_{catalyst}$) QE curve (Fig. 4D, black curve) and the spectral irradiance of the AM 1.5G solar simulator (fig. S10) was also carried out, yielding a STH value of 1.78%, in good agreement (89%) with the direct solar simulator value of 2% (see supplementary material for detailed calculations).

A recent work (40) claimed a STH efficiency of 5.1% for CoO nanoparticles, but the catalyst system was unstable and corroded after 1 hour of

operation. In striking contrast, the CDots- C_3N_4 composite of 1.6×10^{-5} $g_{CDots}/g_{catalyst}$ exhibited long-term stability of at least 200 days for a catalyst dried and reused 200 times (Fig. 3A), whereas the catalyst with the larger CDots concentration of 4.8×10^{-3} $g_{CDots}/g_{catalyst}$ has shown no obvious decay of QE after 50 1-day cycles of reuse (fig. S12). The stability of the CDots- C_3N_4 catalyst system was further studied from several different vantage points: (i) the structural stability of the catalyst over time, (ii) the catalytic functionality (generation rate of H_2 and O_2) over time, (iii) the mass loss or gain after long-term operation, and (iv) the gases released during operation (to detect possible degradation by-products). These factors were probed for two CDots concentrations (1.6×10^{-5} and 4.8×10^{-3} $g_{CDots}/g_{catalyst}$) and two catalyst loads (80 mg/150 ml and 10 mg/150 ml). All photocatalytic water-splitting experiments conducted under different conditions for a variety of reaction times manifested the same H_2 and O_2 generation rates and QEs, within experimental error (Fig. 3A and figs. S12 to S15). These different experiments included (i) 45 days of continuous operation (figs. S13 and S14), (ii) 200 cycles of 24 hours each (Fig. 3A), (iii) 50 cycles of 24 hours each (fig. S12), and (iv) 15 cycles of 24 hours (fig. S15). Raman, FTIR, and XPS spectra (figs. S16 to S18) of CDots- C_3N_4 catalysts before and after 50 24-hour cycled reactions show no obvious differences, confirming the structural stability of the CDots- C_3N_4 catalyst under water-splitting conditions. No CO_2 or N_2 gas could be detected in the reaction system by GC, which suggests that the CDots- C_3N_4 catalyst is stable and did not decompose during the photocatalytic process. There was only negligible mass loss or gain in all the experiments in which the catalyst was weighed before and after use (tables S1 and S2).

A recent U.S. Department of Energy (DOE)-solicited technoeconomical analysis of H_2 generation by solar water splitting (3) suggested that PC systems with STH = 5% (not far away from the 2% efficiency reported above) would allow a H_2 production cost of \$2.30/kg, which meets the DOE target of \$2 to \$4/kg H_2 . The cheapest PE configuration with STH = 10%, in comparison, allows a H_2 production cost of \$5.60/kg H_2 , more than twice the cost of the PC system (although the efficiency of the PE system is twice the efficiency of the PC system). The present PC catalyst thus offers a simpler and cheaper approach to extract H_2 from water in large scale. The main disadvantage of PC systems is the generation of a potentially explosive gas mixture of oxygen and hydrogen, which requires separation to ensure safety. Modern industrial technology offers a variety of mature methods for realization of large-scale hydrogen separation and extraction from other gases (nitrogen, argon, oxygen). This point is considered and is part of the above H_2 production cost evaluation of the DOE-solicited work. The separation systems evaluated (3) include pressure swing adsorption (PSA), temperature swing adsorption (TSA), palladium membrane separation, nanoporous membrane separation, and electrochemical pumps (42).

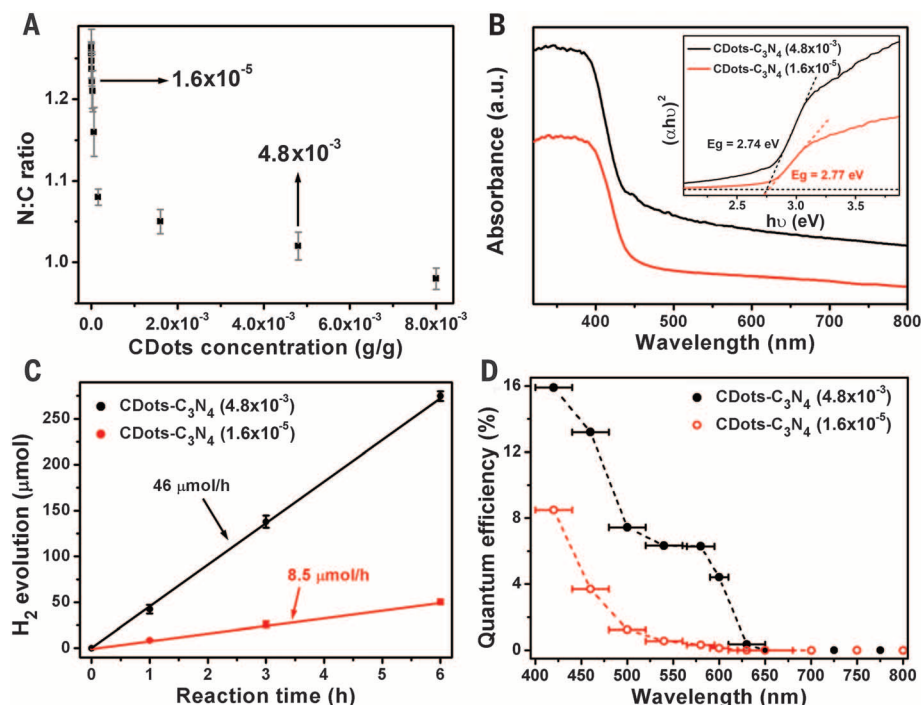


Fig. 4. Catalyst optimization for longer-wavelength absorption. (A) Ratio of nitrogen to carbon (N:C) for different concentrations of CDots ($g_{CDots}/g_{catalyst}$) in the composite catalyst from the average value of the EDS test. (B) Wavelength-dependent absorbance and derived Tauc plots of two different concentrations of CDots in the CDots- C_3N_4 composite (red: 1.6×10^{-5} $g_{CDots}/g_{catalyst}$; black: 4.8×10^{-3} $g_{CDots}/g_{catalyst}$). (C) H_2 generation rate from composites with two different concentrations of CDots (300-W Xe lamp, $\lambda > 420$ nm), showing considerable rate increase for higher CDots concentration. (D) Wavelength-dependent QE of water splitting by catalysts with two different concentrations of CDots applying several bandpass filters (for $\lambda < 680$ nm). A long-pass cutoff filter was used to attain $\lambda > 700$ nm light from a 300-W Xe lamp. For (A) and (C), the vertical error bars indicate the maximum and minimum values obtained; the dot represents the average value. For (D), the horizontal bars indicate the width of the wavelength band of the filters used.

The active wavelength region of CDots-C₃N₄, $\lambda < 620$ nm, would allow a theoretical STH efficiency of ~15% for sunlight (AM 1.5G), which thus leaves substantial room for technical optimization. Our catalyst is also mildly active for the overall seawater photocatalytic splitting. Using CDots-C₃N₄ ($4.8 \times 10^{-3} g_{\text{CDots}}/g_{\text{catalyst}}$) in seawater, we obtained QE (420 nm) of 3.86% and STH = 0.45% (fig. S19). This is a preliminary result, and future studies should probe the reason for the reduction of water-splitting efficiency of sea water versus pure water [QE (420 nm) = 16%, STH = 2%].

We have shown that CDots-C₃N₄ composites can be made of low-cost, environmentally benign materials and can split water into H₂ and O₂ with QEs of 16% for $\lambda = 420 \pm 20$ nm and 6.3% for $\lambda = 580 \pm 15$ nm. The 2.0% STH efficiency obtained is at least one order of magnitude larger than that previously reported for any stable water-splitting photocatalysts (41). It is close to 5% STH, which allows achievement of the DOE price target for H₂ generation. In contrast to the conventional one-step four-electron reaction, CDots-C₃N₄ catalyzes water splitting to hydrogen and oxygen via the stepwise two-electron/two-electron two-step pathway under visible light irradiation. C₃N₄ is responsible for the first step (photocatalysis), and CDots are responsible for the second step (chemical catalysis). CDots also increase the light absorbance and thus the values of QE and STH. The composite nature of the catalyst provides sufficient proximity between the H₂O₂ generation sites on the C₃N₄ surface and the Cdots so that H₂O₂ decomposition and O₂ generation in the second stage become efficient. Moreover, CDots-C₃N₄ maintains a high rate of hydrogen and oxygen production (for $\lambda > 420$ nm) with robust stability in 200 runs of recycling use over 200 days. The results demonstrate CDots-C₃N₄ as a highly efficient and stable photocatalyst for visible light-driven water splitting.

REFERENCES AND NOTES

1. A. Kudo, Y. Miseki, *Chem. Soc. Rev.* **38**, 253–278 (2009).
2. A. Iwase, Y. H. Ng, Y. Ishiguro, A. Kudo, R. Amal, *J. Am. Chem. Soc.* **133**, 11054–11057 (2011).
3. B. A. Pinaud et al., *Energy Environ. Sci.* **6**, 1983–2002 (2013).
4. T. J. Jacobsson, V. Fjällström, M. Sahlberg, M. Edoff, T. Edvinsson, *Energy Environ. Sci.* **6**, 3676–3683 (2013).
5. J. Luo et al., *Science* **345**, 1593–1596 (2014).
6. S. Licht, *J. Phys. Chem. B* **105**, 6281–6294 (2001).
7. M. S. Prévot, K. Sivula, *J. Phys. Chem. C* **117**, 17879–17893 (2013).
8. K. Domen, S. Naito, M. Soma, T. Onishi, K. J. Tamaru, *J. Chem. Soc. Chem. Commun.* **12**, 543–544 (1980).
9. A. Kudo, Y. Miseki, *Chem. Soc. Rev.* **38**, 253–278 (2009).
10. W. J. Youngblood, S. H. A. Lee, K. Maeda, T. E. Mallouk, *Acc. Chem. Res.* **42**, 1966–1973 (2009).
11. K. Maeda, K. Domen, *J. Phys. Chem. Lett.* **1**, 2655–2661 (2010).
12. X. Chen, S. Shen, L. Guo, S. S. Mao, *Chem. Rev.* **110**, 6503–6570 (2010).
13. K. Maeda, *ACS Catal.* **3**, 1486–1503 (2013).
14. K. Maeda et al., *J. Phys. Chem. B* **110**, 13753–13758 (2006).
15. K. Maeda et al., *Nature* **440**, 295 (2006).
16. V. Balzani, A. Credi, M. Venturi, *ChemSusChem* **1**, 26–58 (2008).
17. H. B. Gray, *Nat. Chem.* **1**, 7 (2009).
18. I. Tsuji, H. Kato, A. Kudo, *Angew. Chem. Int. Ed.* **44**, 3565–3568 (2005).
19. J. Liu, Y. Zhang, L. Lu, G. Wu, W. Chen, *Chem. Commun.* **48**, 8826–8828 (2012).
20. F. Rappaport, M. Guergova-Kuras, P. J. Nixon, B. A. Diner, J. Lavergne, *Biochemistry* **41**, 8518–8527 (2002).
21. G. Ananyev, G. C. Dismukes, *Photosynth. Res.* **84**, 355–365 (2005).

22. D. J. Martin, P. J. Reardon, S. J. Moniz, J. Tang, *J. Am. Chem. Soc.* **136**, 12568–12571 (2014).
23. F. He et al., *ACS Appl. Mater. Interfaces* **6**, 7171–7179 (2014).
24. X. Zhang et al., *ACS Catal.* **4**, 162–170 (2014).
25. K. Schwinghammer et al., *J. Am. Chem. Soc.* **136**, 1730–1733 (2014).
26. R. Marschall, *Adv. Mater.* **24**, 2421–2440 (2014).
27. J. Liebig, *Ann. Pharm.* **10**, 10 (1834).
28. S. Yin, Y. Aita, M. Komatsu, T. Sato, *J. Eur. Ceram. Soc.* **26**, 2735–2742 (2006).
29. X. Wang et al., *Nat. Mater.* **8**, 76–80 (2009).
30. B. Chai, T. Peng, J. Mao, K. Li, L. Zan, *Phys. Chem. Chem. Phys.* **14**, 16745–16752 (2012).
31. J. Hong, Y. Wang, Y. Wang, W. Zhang, R. Xu, *ChemSusChem* **6**, 2263–2268 (2013).
32. Q. J. Xiang, J. G. Yu, M. Jaroniec, *J. Phys. Chem. C* **115**, 7355–7363 (2011).
33. A. Suryawanshi et al., *Int. J. Hydrogen Energy* **37**, 9584–9589 (2012).
34. S. Yang et al., *Adv. Mater.* **25**, 2452–2456 (2013).
35. L. Yu et al., *Phys. Chem. Chem. Phys.* **16**, 4106–4114 (2014).
36. H. T. Li, Z. H. Kang, Y. Liu, S. T. Lee, *J. Mater. Chem.* **22**, 24230–24253 (2012).
37. H. Ming et al., *Dalton Trans.* **41**, 9526–9531 (2012).
38. X. Wang et al., *J. Am. Chem. Soc.* **131**, 1680–1681 (2009).
39. M. Yang, Q. Huang, X. Q. Jin, *Mater. Sci. Eng. B* **177**, 600–605 (2012).

40. L. Liao et al., *Nat. Nanotechnol.* **9**, 69–73 (2014).
41. S. Mubeen et al., *Nat. Nanotechnol.* **8**, 247–251 (2013).
42. R. W. Baker, *Ind. Eng. Chem. Res.* **41**, 1393–1411 (2002).

ACKNOWLEDGMENTS

We thank A. Rothschild for helpful discussions. We thank Beijing and Shanghai synchrotron radiation facility for XANES and EXAFS data collection. Supported by Collaborative Innovation Center of Suzhou Nano Science and Technology, the National Basic Research Program of China (973 Program) (2012CB825803, 2013CB932702), the National Natural Science Foundation of China (51422207, 51132006, 21471106), the Specialized Research Fund for the Doctoral Program of Higher Education (20123201110018), a Suzhou Planning Project of Science and Technology (ZXG2012028), and a project funded by the Priority Academic Program Development of Jiangsu Higher Education Institutions (PAPD).

SUPPLEMENTARY MATERIALS

www.sciencemag.org/content/347/6225/970/suppl/DC1
Materials and Methods
Figs. S1 to S36
Tables S1 to S3
References (43–54)

17 November 2014; accepted 26 January 2015
10.1126/science.aaa3145

PLASMA PHYSICS

Stochastic electron acceleration during spontaneous turbulent reconnection in a strong shock wave

Y. Matsumoto,^{1*} T. Amano,² T. N. Kato,³ M. Hoshino²

Explosive phenomena such as supernova remnant shocks and solar flares have demonstrated evidence for the production of relativistic particles. Interest has therefore been renewed in collisionless shock waves and magnetic reconnection as a means to achieve such energies. Although ions can be energized during such phenomena, the relativistic energy of the electrons remains a puzzle for theory. We present supercomputer simulations showing that efficient electron energization can occur during turbulent magnetic reconnection arising from a strong collisionless shock. Upstream electrons undergo first-order Fermi acceleration by colliding with reconnection jets and magnetic islands, giving rise to a nonthermal relativistic population downstream. These results shed new light on magnetic reconnection as an agent of energy dissipation and particle acceleration in strong shock waves.

The acceleration of charged particles is a fundamental topic in astrophysical, space, and laboratory plasma research. Very high-energy particles are commonly found in astrophysical and planetary shocks (1–3) and in the energy releases of solar flares and terrestrial substorms (4–7). Collisionless shock waves and magnetic reconnection, respectively, have been considered to be the ultimate plasma energization mechanisms responsible for relativistic particles found in such phenomena. Although ions can be energized efficiently during

the energy conversions, plasma kinetic processes in a localized region must be invoked to explain the observed electron heating and acceleration (8–11). In this Report, we show that efficient electron energization can occur during turbulent magnetic reconnection that arises over an entire region of a strong shock wave.

Magnetized collisionless shocks are characterized by the Alfvén Mach number M_A , which is the ratio of the flow speed to the Alfvén speed. When the Alfvén Mach number becomes larger than a critical value ($M_A^* \sim 3$), the upstream (low-entropy) plasma cannot be fully dissipated across the shock (12). In such supercritical collisionless shocks, ions are partly reflected by the shock front and then counterflow in the upstream region. The motion of these particles serves to dissipate the plasma further by exciting multiple kinetic instabilities (13). The reflected ions are the key

¹Department of Physics, Chiba University 1-33 Yayoi-cho, Inage-ku, Chiba 263-8522, Japan. ²Department of Earth and Planetary Science, The University of Tokyo, 7-3-1 Hongo, Bunkyo-ku, Tokyo 113-0033, Japan. ³Center for Computational Astrophysics, National Astronomical Observatory of Japan, 2-21-1 Osawa, Mitaka, Tokyo 181-8588, Japan.

*Corresponding author. E-mail: ymatumot@chiba-u.jp

This copy is for your personal, non-commercial use only.

If you wish to distribute this article to others, you can order high-quality copies for your colleagues, clients, or customers by [clicking here](#).

Permission to republish or repurpose articles or portions of articles can be obtained by following the guidelines [here](#).

The following resources related to this article are available online at www.sciencemag.org (this information is current as of February 26, 2015):

Updated information and services, including high-resolution figures, can be found in the online version of this article at:

<http://www.sciencemag.org/content/347/6225/970.full.html>

Supporting Online Material can be found at:

<http://www.sciencemag.org/content/suppl/2015/02/25/347.6225.970.DC1.html>

This article **cites 54 articles**, 2 of which can be accessed free:

<http://www.sciencemag.org/content/347/6225/970.full.html#ref-list-1>

This article appears in the following **subject collections**:

Chemistry

<http://www.sciencemag.org/cgi/collection/chemistry>